Thomas-Fermi simulations of dense plasmas without pseudopotentials

C. E. Starrett

Phys. Rev. E **96**, 013206 — Published 12 July 2017

DOI: 10.1103/PhysRevE.96.013206

Thomas-Fermi simulations of dense plasmas without pseudopotentials

C. E. Starrett[1, *]

[1]*Los Alamos National Laboratory, P.O. Box 1663, Los Alamos, NM 87545, U.S.A.*

(Dated: June 19, 2017)

The Thomas-Fermi model for warm and hot dense matter is widely used to predict material properties such as the equation of state. However, for practical reasons current implementations use pseudopotentials for the electron-nucleus interaction instead of the bare Coulomb potential. This complicates the calculation and quantities such as Free energy cannot be converged with respect to the pseudopotential parameters. We present a method that retains the bare Coulomb potential for the electron-nucleus interaction and does not use pseudopotentials. We demonstrate that accurate Free energies are obtained by checking variational consistency. Examples for aluminum and iron plasmas are presented.

Keywords: Thomas-Fermi simulation, warm dense matter, pseudopotential

I. INTRODUCTION

Orbital Free, and in particular Thomas-Fermi, simulations of warm and hot dense matter are widely used to calculate material properties such as equation of state and ionic transport coefficients [1–7]. These simulations all rely on the pseudopotential approximation, in which the electron-nucleus interaction potential $-Z/r$ (where Z is the nuclear charge) is replaced by a pseudopotential below some cutoff radius [2, 5]. The motivation for this arises when one wishes to solve the equations of the Orbital Free model. This involves solving the Poisson equation, which is usually done in Fourier space using Fast Fourier Transforms (FFTs). The FFT technique requires that the electron density be resolved on a uniformly spaced spatial grid. However, the strong attraction between the nuclei and electrons leads to a pile-up of electrons near the nuclei that typically cannot be resolved on such a grid. Hence, one replaces the strong electron-nucleus potential with a pseudopotential that smoothes out the electron density near the nuclei, allowing it to be accurately represented on the uniform grid. Clearly, this must be done carefully so as not to significantly influence the property that one is trying to calculate, and convergence tests must be carried out with respect to pseudopotential parameters. For the pressure it has been shown that convergence with respect to the pseudopotential cutoff radius can be achieved [1]. However, it was not possible to achieve convergence with respect to internal energy [1]. Thus, for practical as well as aesthetic reasons it is desirable to avoid the use of pseudopotentials.

In this work we present a method that allows solution of the Thomas-Fermi model without recourse to the pseudopotential approximation. The method relies on a numerical trick that decomposes the electron density into a sum of spherically symmetric densities and a remainder. The key point is that the spherically symmetric densities are accurate near the nuclei so that the remainder density can be accurately represented on a uniformly spaced spatial grid. The Poisson equation can then be solved in two steps: 1) the part due to the spherically symmetric densities can be easily solved using an established and rapid technique, and 2) the contribution from the remainder density can be solved using the usual FFT method.

While the present work is limited in application to the Thomas-Fermi model, the method is equally applicable to other Orbital-Free functionals. The Thomas-Fermi model is a widely used but simple model. In principle it is correct only where the electron density is uniform. However, in practice pressures and ionic transport coefficients are quite reasonable from moderate to high temperatures in the compressed matter regime [3, 6].

The structure of this paper is as follows. First, in section II we review and define the Thomas-Fermi model, including the thermodynamic quantities. We use this section to introduce a test of the model: two expressions for the pressure are given, on the one hand the pressure is evaluated using a virial expression, on the other the pressure is evaluated using a numerical derivative of the Free energy. Both pressures should be equal to within numerical tolerances provided the method is truly minimizing the Grand potential, as required by density functional theory [8]. This condition would not be satisfied if a pseudopotential were to be used for example. In section III we describe the trick that allows one to avoid the use of pseudopotentials and discuss other numerical issues that arise when not using pseudopotentials. We also give our algorithm for solution of the model. In section IV we show examples for aluminum and iron plasmas, and explicitly demonstrate the equivalence of the virial and thermodynamic routes to the pressure for simple cubic aluminum. We also compare pressure for a solid density aluminum plasma to an average atom model. Lastly, in section V we draw our conclusions. Unless otherwise stated, Hartree atomic units are used throughout in which $\hbar = m_e = e = k_B = 1$.

*Electronic address: starrett@lanl.gov

II. REVIEW OF THE THOMAS-FERMI MODEL

We consider N nuclei at positions $\{R_i\}$ in a cubic computational volume V with periodic boundary conditions. The total free energy F is

$$F = F^I + F_e^{TF} + F_{ee}^{xc} + F^{el} \tag{1}$$

where F^I is the ideal ion contribution, F_e^{TF} is the Thomas-Fermi kinetic and entropic term

$$F^{\rm TF} = \frac{1}{\beta}\int_V d^3r\,\left(n_{\rm e}(\boldsymbol{r})\eta(\boldsymbol{r}) - \frac{2}{3}c_{\rm TF}I_{3/2}\left[\eta(\boldsymbol{r})\right]\right) \tag{2}$$

with $\beta = 1/T$ the inverse temperature, I_j is the Fermi integral of order j (see [9]),

$$c_{\rm TF} \equiv \frac{\sqrt{2}}{\pi^2\beta^{3/2}}. \tag{3}$$

and

$$n_e(\boldsymbol{r}) = c_{TF}I_{1/2}\left[\eta(\boldsymbol{r}))\right] \tag{4}$$

is the electron density. $\eta(\boldsymbol{r})$ is found by requiring the grand potential to be at a minimum with respect to $n_e(\boldsymbol{r})$ (see equation (13)).

F^{xc} is the exchange and correlation free energy

$$F_{ee}^{xc} = \int_V d^3r\, f_{ee}^{xc}\left[n_e(\boldsymbol{r})\right] \tag{5}$$

where throughout this work we have used the zero temperature local density approximation [10] (which ignores correlation effects),

$$f_{ee}^{xc}[n] = -\frac{3}{4}\left(\frac{3}{\pi}\right)^{\frac{1}{3}} n^{\frac{4}{3}} \tag{6}$$

The corresponding exchange and correlation potential is

$$V_{ee}^{xc}(\boldsymbol{r}) = \frac{\delta F_{ee}^{xc}}{\delta n_e} = \left(\frac{3n_e(\boldsymbol{r})}{\pi}\right)^{\frac{1}{3}} \tag{7}$$

Lastly in equation (1), F^{el} is the electrostatic free energy [1]

$$F^{el} = \frac{1}{2}\int_V d^3r\,\left(n_e(\boldsymbol{r})V^{el}(\boldsymbol{r}) - \sum_{i=1}^{N} Z_i\delta(\boldsymbol{r}-\boldsymbol{R}_i)\bar{V}_i(\boldsymbol{r})\right) \tag{8}$$

where the electrostatic potential $V^{el}(\boldsymbol{r})$ is

$$V^{el}(\boldsymbol{r}) = -\sum_{i=1}^{\infty}\frac{Z_i}{|\boldsymbol{r}-\boldsymbol{R}_i|} + \int d^3r'\frac{n_e(\boldsymbol{r}')}{|\boldsymbol{r}-\boldsymbol{r}'|} \tag{9}$$

[1] The sum over nuclei in equation (8) is restricted to the N particles in volume V.

and $\bar{V}_j$ is

$$\begin{aligned}\bar{V}_j(\boldsymbol{r}) &= -\sum_{i=1,i\neq j}^{\infty}\frac{Z_i}{|\boldsymbol{r}-\boldsymbol{R}_i|} + \int d^3r'\frac{n_e(\boldsymbol{r}')}{|\boldsymbol{r}-\boldsymbol{r}'|} \\ &= V^{el}(\boldsymbol{r}) + \frac{Z_j}{|\boldsymbol{R}_j-\boldsymbol{R}_i|}\end{aligned} \tag{10}$$

The grand potential Ω is related to the Free energy via

$$\Omega = F - \mu\int_V d^3r\, n_e(\boldsymbol{r}) \tag{11}$$

where μ is the electronic chemical potential and serves as Lagrange multiplier to ensure the computational volume is charge neutral. Ω is required to be at a minimum with respect to variations in the electron density

$$\frac{\delta\Omega}{\delta n_e(\boldsymbol{r})} = 0 \tag{12}$$

which yields

$$\eta(\boldsymbol{r}) = \beta\left(\mu - V^{el}(\boldsymbol{r}) - V_{ee}^{xc}(\boldsymbol{r})\right) \tag{13}$$

The self-consistent solution to equations (4), (7), (9) and (13), with μ determined by charge neutrality, and for a given set of nuclear positions $\{\boldsymbol{R}_i\}$, defines the Thomas-Fermi model. Variations of this model for different exchange and correlation potentials are easily constructed.

The pressure is given by

$$P = -\left.\frac{\partial F}{\partial V}\right|_T \tag{14}$$

Using the virial theorem, the pressure is given by [11]

$$P\,V = \frac{2}{3}K_e^{TF} + \frac{2}{3}K^I + \frac{1}{3}F^{el} + C^{xc} \tag{15}$$

where C^{xc} is the contribution from exchange and correlation,

$$C^{xc} = -F_{ee}^{xc} + \int_V d^3r\, n_e(\boldsymbol{r})\frac{\delta F_{ee}^{xc}}{\delta n_e(\boldsymbol{r})}. \tag{16}$$

K_e^{TF} is

$$K_e^{TF} = \frac{1}{\beta}\int_V d^3r\, c_{TF}I_{3/2}\left[\eta(\boldsymbol{r})\right] \tag{17}$$

and K^I is the ideal ion contribution. We will refer to the pressure that is given by equation (14) where the derivative is carried out numerically as the thermodynamic pressure P^{th}, and the pressure evaluated with equation (15) as the Virial pressure P^{vir}. If the numerical calculation is accurate then the two pressures are the same

$$P^{vir} = P^{th} \tag{18}$$

This provides a stringent test on the numerical implementation.

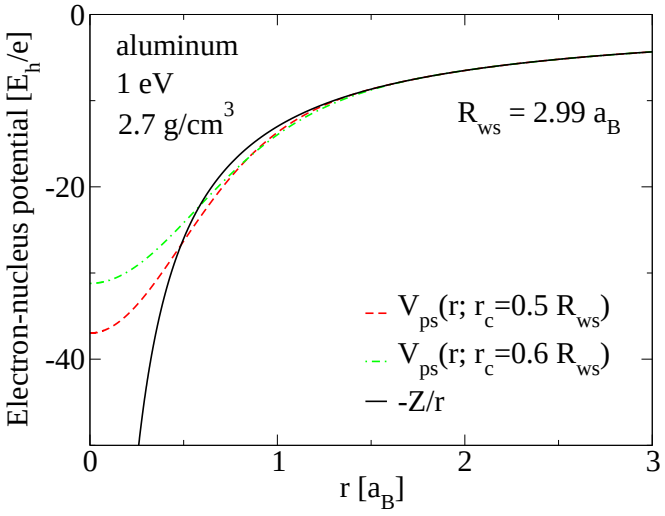

FIG. 1: (Color online) Example of a typical pseudopotential, using the method of reference [2]. The Coulomb potential $-Z/r$ is replaced by a pseudopotential $V_{ps}(r)$ below some cutoff radius r_c. Calculated properties should be converged with respect to pseudopotential parameters, in this case r_c.

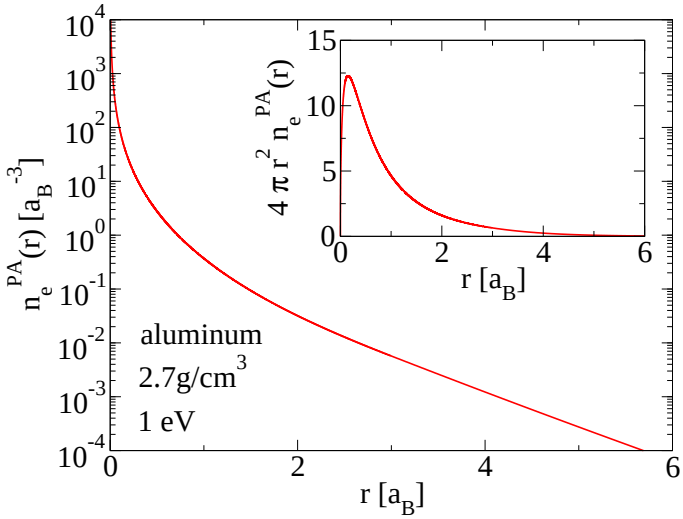

FIG. 2: (Color online) Example of a $n_e^{PA}(r)$ for solid density aluminum at 1 eV generated by the model of references [12, 13]. The inset shows the same electron density but multiplied by $4\pi r^2$. $n_e^{PA}(r)$ is an accurate approximation to the full 3-dimensional electron density near the nuclei, a fact guaranteed by realization that the effective potential felt by the electrons near the nuclei is dominated by the Coulomb nuclear potential.

III. PSEUDOPOTENTIALS AND HOW TO AVOID USING THEM

The self-consistent solution of the TF model requires evaluation of the Poisson equation (equation (9)). This is usually solved using Fast Fourier Transforms (FFT). In this method the electron density is calculated on a equally spaced grid and Fourier Transformed ($\mathscr{F}$)

$$\mathscr{F}[n_e(\boldsymbol{r})] = \tilde{n}_e(\boldsymbol{k}) \tag{19}$$

The potential is then found via the inverse Fourier Transform ($\mathscr{F}^{-1}$)

$$V^{el}(\boldsymbol{r}) = -\sum_{i=1}^{\infty} \frac{Z_i}{|\boldsymbol{r}-\boldsymbol{R}_i|} + \mathscr{F}^{-1}\left[\frac{4\pi}{k^2}\tilde{n}_e(\boldsymbol{k})\right] \tag{20}$$

This presents a numerical challenge because the electron density $n_e(\boldsymbol{r})$ must be accurately resolved on the equally spaced grid. Due to electron pile-up near the nuclei this is impractical for most cases. The usual solution is to replace the electron-nucleus Coulomb potential with a pseudopotential that prevents this pile-up. But for the reasons discussed earlier this is undesirable. An example of a typical pseudopotential is given in figure 1.

To avoid using a pseudopotential one can reformulate equation (9) using an exact decomposition proposed in reference [14]. One starts by approximating the total electron density as a superposition of spherically symmetric densities that we call pseudoatom densities $n_{e,i}^{PA}(r)$. These densities are designed to be accurate representations of the full electron density near the nuclei where the potential is dominated by the nucleus. Each $n_{e,i}^{PA}(r)$ is required to satisfy charge normalization, i.e.

$$\int d^3r\, n_{e,i}^{PA}(r) = Z_i. \tag{21}$$

The integral is over all space but converges as the pseudoatom densities go to zero faster than r^2. The superposition electron density is then

$$n_e^{super}(\boldsymbol{r}) = \sum_{i=1}^{\infty} n_{e,i}^{PA}(|\boldsymbol{R}_i - \boldsymbol{r}|) \tag{22}$$

There is no unique definition of $n_{e,i}^{PA}(r)$ and a number of reasonable ways to calculate it can be proposed, provided they satisfy the above constraints. We have used the physically motivated definition given in references [12, 13]. This method is fast (a few seconds) and robust. We note however, that the method presented here is not restricted to using the model of [12, 13], and other methods to generate $n_{e,i}^{PA}(r)$ can be envisaged (see below). An example of a $n_{e,i}^{PA}(r)$ is given in figure 2. Finally, we point out that the pseudoatom densities can and do overlap spatially in equation (22) and that is causes no problem.

Using $n_e^{super}(\boldsymbol{r})$, the total electron density is

$$n_e(\boldsymbol{r}) = n_e^{super}(\boldsymbol{r}) + \Delta n_e(\boldsymbol{r}) \tag{23}$$

and equation (9) is rewritten

$$V^{el}(\boldsymbol{r}) = V^{super}(\boldsymbol{r}) + \Delta V(\boldsymbol{r}) \tag{24}$$

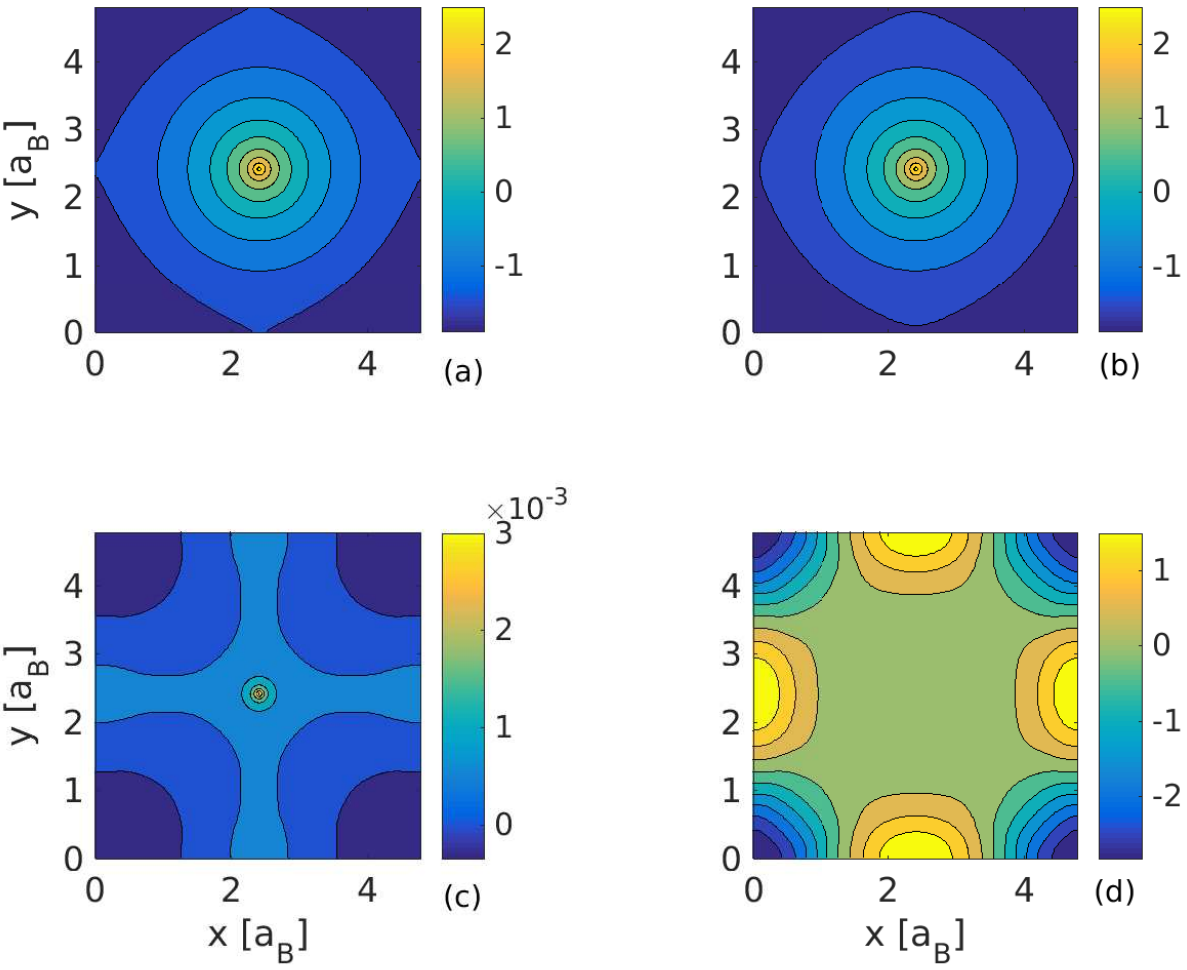

FIG. 3: (Color online) 2-dimensional slice of electron densities in a cubic volume for simple cubic aluminum at 1 eV and solid density. The slice is taken though a crystal plane with an atom at the center. (a) full electron density $\log_{10} n_e(\boldsymbol{r})$ [a_B^3]; (b) electron density from superposition approximation $\log_{10} n_e^{super}(\boldsymbol{r})$ [a_B^3]; (c) absolute difference $\Delta n_e(\boldsymbol{r}) = n_e(\boldsymbol{r}) - n_e^{super}(\boldsymbol{r})$ [a_B^3]; (d) percentage difference $\Delta n_e(\boldsymbol{r})/n_e(\boldsymbol{r})$.

where

$$V^{super}(\boldsymbol{r}) = \sum_{i=1}^{\infty} V_i^{PA}(|\boldsymbol{r} - \boldsymbol{R}_i|) \tag{25}$$

and

$$\Delta V(\boldsymbol{r}) = \int d^3r' \frac{\Delta n_e(\boldsymbol{r}')}{|\boldsymbol{r} - \boldsymbol{r}'|} \tag{26}$$

with

$$V_i^{PA}(r) = -\frac{Z_i}{r} + \int d^3r' \frac{n_{e,i}^{PA}(r')}{|\boldsymbol{r} - \boldsymbol{r}'|} \tag{27}$$

$V_i^{PA}(r)$ is straightforward and rapid to evaluate using the well known and widely used spherical harmonic expansion of $1/|\boldsymbol{r}-\boldsymbol{r}'|$ and a non-uniform radial grid. While the sum in equation (25) is formally to infinity, in practice only a finite number of terms need be included. $V^{super}(\boldsymbol{r})$ is periodic and only those $V_i^{PA}(|\boldsymbol{r}-\boldsymbol{R}_i|)$ with appreciable magnitude inside the computational volume contribute to the summation.

Since $n_e^{super}(\boldsymbol{r})$ is designed to be accurate near the nuclei, $\Delta n_e(\boldsymbol{r})$ does not have any strong gradients associated with electron pile-up near the nuclei in it. It is therefore amenable to the FFT technique which requires uniformly space grids. The total potential V^{el} is thus calculated by constructing $V^{super}(\boldsymbol{r})$ on the uniform grid and calculating $\Delta V(\boldsymbol{r})$ with FFT's. This solves the major challenge in removing the pseudopotential.

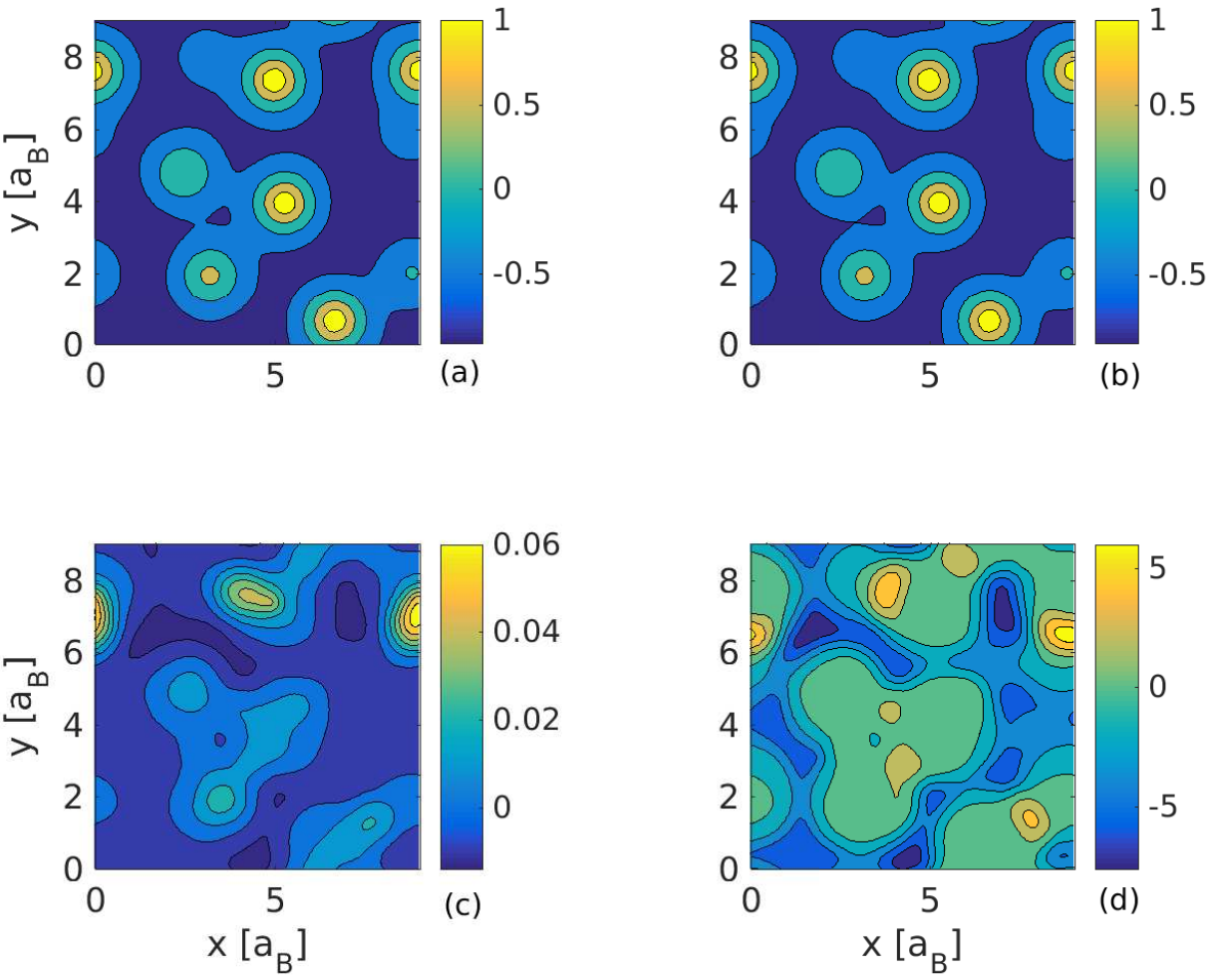

FIG. 4: (Color online) 2-dimensional slice of electron densities in a cubic volume for a snapshot of an iron plasma simulation at 10 eV and 22.5 g/cm^3 with 27 atoms in the simulation cell. (a) full electron density $\log_{10} n_e(\boldsymbol{r})$ [a$_\mathrm{B}^3$]; (b) electron density from superposition approximation $\log_{10} n_e^{super}(\boldsymbol{r})$ [a$_\mathrm{B}^3$]; (c) absolute difference $\Delta n_e(\boldsymbol{r}) = n_e(\boldsymbol{r}) - n_e^{super}(\boldsymbol{r})$ [a$_\mathrm{B}^3$]; (c) percentage difference $\Delta n_e(\boldsymbol{r})/n_e(\boldsymbol{r})$. Note the considerably reduced range of $\Delta n_e(\boldsymbol{r})$ compared to $n_e(\boldsymbol{r})$.

The remaining challenge is how to evaluate integrals of the type

$$\int_V d^3r\, n_e(\boldsymbol{r}) \tag{28}$$

that are required when solving for μ, or

$$\int_V d^3r\, I_{3/2}[\eta(\boldsymbol{r})] \tag{29}$$

that are required when calculating the thermodynamic properties. To carry out these integrals we have tested two methods. First is a numerical trick similar to that used for solving the Poisson equation. Instead of evaluating (28) directly, we numerically evaluate on the uniformly spaced spatial grid

$$\int_V d^3r\, \left(n_e(\boldsymbol{r}) - n_e^{super}(\boldsymbol{r})\right) \tag{30}$$

which is accurate because the integrand does not have strong gradients, and then add the contribution from $n_e^{super}(\boldsymbol{r})$ back in. This latter is easy to calculate as it is the sum of spherically symmetric quantities. The same method can be used for the other integrals like equation (29) if we define suitable spherically symmetric quantities for each integral. This trick was used successfully in reference [14] for the pseudo-atom molecular dynamics (PAMD) model. The disadvantage of this method is

T [eV]	P_{ex}^{th} [Mbar]	P_{ex}^{vir} [Mbar]	ΔP [%]	F_{ex} [E_h]	ΔF_{ex} [E_h]
1	0.3701	0.3635	-1.8	-321.866334	-0.000141
2	0.4687	0.4627	-1.28	-321.944525	-0.000179
5	0.9946	0.9907	-0.4	-322.452406	-0.000380
10	2.326	2.324	-0.0584	-324.035145	-0.000889
15	4.058	4.059	0.0201	-326.355184	-0.001551
20	6.116	6.119	0.0397	-329.291693	-0.002338
30	11.05	11.05	0.049	-336.726635	-0.004222
40	16.89	16.9	0.0446	-345.934585	-0.006454
50	23.49	23.5	0.0352	-356.662173	-0.008979
60	30.76	30.77	0.0273	-368.729337	-0.011755
70	38.59	38.6	0.0253	-381.998297	-0.014750
80	46.94	46.94	0.0192	-396.359225	-0.017938
90	55.73	55.73	0.0148	-411.721118	-0.021298
100	64.92	64.92	0.0105	-428.007640	-0.024811

TABLE I: Thermodynamic accuracy for simple cubic aluminum at 2.7g/cm^3. The thermodynamical excess pressure P_{ex}^{th} is calculated by numerical derivative of the excess free energy F_{ex}. Here we use a 0.1% centered difference (i.e. $\Delta V = 0.1\%$ of V). ΔF_{ex} is the difference $F_{ex}(V+\Delta V) - F_{ev}(V)$. At 1 eV, a 1% accuracy in P_{ex}^{th} requires F_{ex} to be accurate to the 9^{th} significant figure. This is therefore a very stringent test of the numerics. $\Delta\tilde{P}[\%]$ is the percentage difference between P_{ex}^{th} and P_{ex}^{vir}.

that one is more tied to the model [12, 13] to accurately calculate the necessary spherically symmetric quantities, though, as for $n_{e,i}^{PA}(r)$, other approaches to generate these can be envisaged.

An alternative approach is to design an integration scheme that accurately solves integrals like equations (28) and (29) directly. We have implemented a method that tessellates space into Voronoi polyhedra using the code of reference [15]. Integrals inside each polyhedra a partitioned into a region of an inscribed sphere treated numerically with spherical polar coordinates (where spherical symmetry is not assumed), and a second region of the remaining space. This remaining space can be accurately integrated using the iso-parametric integration technique of reference [16]. We note that reference [16] uses a transform to a cube which we found to be problematic for certain complicated geometries. This was easily remedied by transforming to a prism instead. The advantage to this method is that it is independent of the model [12, 13]. However, it does require interpolation between the uniform mesh on which $\Delta V(\boldsymbol{r})$ is calculated by FFT and the non-uniform grid used for the integration. As a consequence we found it to be significantly more costly to evaluate. We have checked that both approaches yield the same results to within numerical tolerances.

With these two impediments solved one can proceed with the pseudopotential free Thomas-Fermi simulations. Our algorithm for solving the TF self-consistent field is as follows:

1. Solve for $n_{e,i}^{PA}(r)$ and calculate $V_i^{PA}(r)$

2. With nuclear positions given, construct $n_e^{super}(\boldsymbol{r})$ and $V_e^{super}(\boldsymbol{r})$. Use these as initial guesses for the self-consistent field scheme.

3. Solve for the electron density $n_e(\boldsymbol{r})$ using equation (4). Adjust μ until the computational cell is charge neutral. This involves evaluating the integral
$$\int_V d^3r\, n_e(\boldsymbol{r})$$

4. Solve the Poisson equation for $V^{el}(\boldsymbol{r})$ using method discussed above, and calculate $V_{ee}^{xc}(\boldsymbol{r})$.

5. Check for convergence. If not converged, linearly mix new potential with the old and go back to step 3. Cycle until converged.

This algorithm is significantly different from that used by others, for example [17]. It has the advantage of guaranteeing a positive electron density without a change of variables. It may however take more self-consistent field steps. A detailed comparison of the above algorithm and that used by others has not yet been carried out.

Finally, we note that the method of calculating $F^{el}(\boldsymbol{r})$ has a significant advantage over other more traditional approaches as it does not require an Ewald summation [18]. Usually the calculation of the ion-ion energy requires one to use the Ewald summation trick [17] that introduces an artificial screening distribution to allow rapid summation in real space, and then subtracts out this screening charge in Fourier space. One can think of our decomposition method as using the $n_{e,i}^{PA}(r)$ as the screening charge in real-space, allowing rapid summation. However, as this screening charge is not artificial (in the

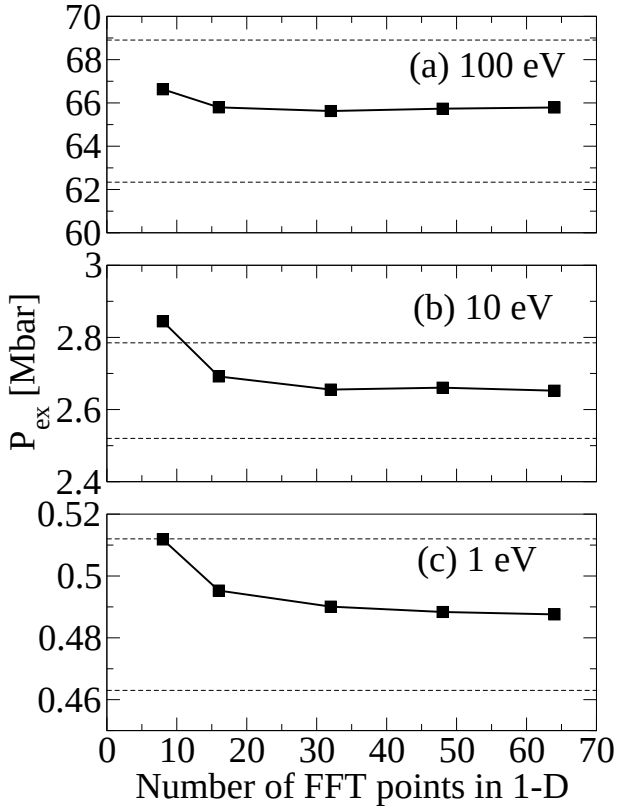

FIG. 5: (Color online) Convergence of excess pressure P_{ex}^{vir} with respect to number of FFT points in one dimension N. The total number of FFT points is N^3. Convergence is shown for solid density aluminum at three temperatures. The horizontal dashed lines indicate ±5% from the converged value.

Ewald sense) it does not need to be subtracted out in Fourier space.

IV. NUMERICAL RESULTS

In figure 3 we show a 2-dimensional slice of electron densities for simple cubic[2] aluminum at solid density and 1 eV. The atom is at the center of the box and lies in the plane of the slice shown. In the top left panel is the converged electron density $n_e(\boldsymbol{r})$. The build up of electrons near the nucleus is apparent (note we show the log of the electron density). Formally $n_e(\boldsymbol{r})$ diverges as $r^{-3/2}$ as $r \to 0$, where r is the radial distance from a nucleus. Such divergences are not resolved on the uniform grid used to plot $n_e(\boldsymbol{r})$. The electron density from the superposition approximation $n_e^{super}(\boldsymbol{r})$ is shown in the top right, and the difference between it and the converged electron density is shown in the lower left. Clearly $n_e^{super}(\boldsymbol{r})$ is quite close to the converged electron density. The largest absolute differences occur near the nucleus. However, due to the very large values of $n_e(\boldsymbol{r})$ near the nucleus these differences probably just reflect the numerical tolerances. In the bottom right panel we show the percentage relative difference. This shows that $n_e^{super}(\boldsymbol{r})$ is very accurate near the nucleus, as expected, and that it underestimates the $n_e(\boldsymbol{r})$ in the region between the central atom and the nearest atoms (i.e. at (±1,0,0), (0,±1,0) and (0,0,±1) if the central atom is at (0,0,0)), and overestimates the electron density in the regions between the remaining nearest neighbors. However, the relative differences are rather small, remaining below 3% everywhere.

In figure 4 we show a 2-dimensional slice of the electron densities for a snapshot of an iron simulation at 10 eV and 22.5 g/cm^3. We have taken the ion positions from the PAMD code [19]. Again the superposition density is close to the converged electron density, with differences up to $\approx 6\%$ observed. Further, we again see that $n_e^{super}(\boldsymbol{r})$ underestimates the electron density between two close neighbors, and overestimates it elsewhere. This indicates that the Thomas-Fermi model drives electrons into the regions where the total nuclear potential $\sum_i -Z_i/|\boldsymbol{r}-\boldsymbol{R}_i|$ is most attractive – an effect beyond the superposition approximation.

In both figures 3 and 4 it is apparent why the method to solve the Poisson equation works. The bottom left panel of both figures shows $\Delta n_e(\boldsymbol{r})$ that must be Fourier transformed with FFT's. It is clear that the strong gradients near the nuclei are eliminated and only a relatively slowing varying quantity remains that is accurately represented on a uniform grid. We have also checked that a significantly different pseudoatom density $n_{e,i}^{PA}(r)$ results in the same answer, i.e. we modified $n_{e,i}^{PA}(r)$ so that its normalization was maintained, but its behavior away from the nuclei was significantly changed, and the final $n_e(\boldsymbol{r})$, P and F were not significantly different. This also confirms that one need not use the model of references [12, 13] to generate $n_{e,i}^{PA}(r)$, though it certainly serves as an excellent choice.

In table I we check the thermodynamic consistency of the method. The pressure P_{ex}^{th} is calculated using a numerical derivative in equation (14), while P_{ex}^{vir} is calculated using equation (15). Excess ("ex") quantities are reported that do not include the ideal ion contribution (eg. $F_{ex} = F - F^I$). If the numerics were perfect we would have $P_{ex}^{th} = P_{ex}^{vir}$. Table I focuses on simple cubic aluminum at solid density over a range of temperatures. Clearly, the method is very accurate with the largest relative difference being at the lower temperature due to relatively the small pressure. The table also demonstrates that highly accurate (to the 9^{th} significant figure) Free energies are required to evaluate P^{th}. To achieve this numerical accuracy we used 128^3 Fourier transform grid points, which is quite a lot. Fortunately, P^{vir} is much less sensitive to the accuracy and one can get away with a much smaller number of grid points (eg. 32^3 is more than enough for this case).

[2] We use simple cubic crystal structure purely for simplicity.

T [eV]	AA P_{ex} [Mbar]	SC P_{ex} [Mbar]	ΔP [%]	MD P_{ex} [Mbar]	ΔP [%]
1	0.299	0.3635	21.6	0.4915	64.4
2	0.4005	0.4627	15.5	0.65	62.3
5	0.9339	0.9907	6.08	1.266	35.6
10	2.267	2.324	2.53	2.65	16.9
15	3.999	4.059	1.48	4.423	10.6
20	6.058	6.119	0.998	6.517	7.58
30	10.99	11.05	0.541	11.48	4.47
40	16.84	16.9	0.326	17.37	3.14
50	23.46	23.5	0.199	24.02	2.4
60	30.73	30.77	0.115	31.33	1.96
70	38.58	38.6	0.0549	39.23	1.69
80	46.94	46.94	0.00827	47.64	1.48
90	55.75	55.73	-0.0262	56.5	1.35
100	64.96	64.92	-0.0562	65.77	1.24

TABLE II: Excess pressure of average atom (AA) model compared to simple cubic (SC) and disordered (MD) simulations for aluminum at 2.7 g/cm^3. For the disordered case we have taken the ion positions from corresponding PAMD simulations [19]. ΔP [%] is the percentage difference relative to the AA pressure [14].

The agreement of P^{vir} and P^{th} is a strong verification of the method and its implementation, and to our knowledge is the first time that such an calculation has been reported as it is not possible if pseudopotentials are used.

In table II we show pressures for solid density aluminum from three pseudopotential free calculations. The first is the widely used average atom model [20], labeled AA. In the middle two columns this is compared to simple cubic calculations with the present method, labeled SC. Above 20 eV the two models are in close agreement. Below this temperature, the SC pressure is consistently larger than the AA. This indicates that in the SC model electrons redistribute themselves from higher density regions near the nuclei to lower density areas, and therefore increase the pressure. This effect is restricted in the AA model because all screening must occur within the ion sphere. At higher temperatures the electrons have more energy on average and are therefore less sensitive to the nuclear positions.

In the right hand two columns of table II we compare pressures of disordered plasmas, labeled MD, to the AA model. We have taken the nuclear positions from the PAMD model [19]. It is worth noting that it is possible to obtain nuclear positions self-consistently in the present approach using Born-Oppenheimer Molecular Dynamics [2], but we have not yet implemented this. The pressures from the MD model have been compared to previous TF-MD simulations that used pseudopotential [19] and were found to be in good agreement (differences of less than $\approx$ 2 %). We used 64 particles in the simulation box, and 64^3 FFT grid points. The time step depends on the temperature and we used to method of reference [1] to aid in its determination. The effect of the ionic disorder is to further increase the pressure relative to the AA model. Beyond 50 eV AA and MD pressures are with $\approx$ 2 % of each other.

In figure 5 we show convergence of the excess pressure as a function of number of FFT points for solid density aluminum at three temperatures. We consider the pressure using ion positions from PAMD with 64 atoms in the cell. In all cases the pressure is well converged using 32^3 points.

V. CONCLUSIONS

An accurate method that allows the solution of the Thomas-Fermi model without the pseudopotential approximation has been presented. The method was demonstrated for aluminum and iron plasmas, and verified to give thermodynamically consistent results for simple cubic aluminum. This serves as a strong test of the method and its numerical implementation. Calculations of pressure for aluminum plasmas were compared to average atom results, elucidating the influence of ionic structure. Lastly, we note that the method is expected to work for other orbital free functionals such as the von Weiszäcker term [21]. The approach presented here should be straightforward to implement in existing TFMD codes [1, 2, 17, 21].

Acknowledgments

The author thanks D. Saumon and T. Sjostrom for useful conversations about this work. This work was per-

formed under the auspices of the United States Department of Energy under contract DE-AC52-06NA25396 and LDRD number 20150656ECR.

[1] J.-F. Danel, L. Kazandjian, and G. Zérah. Equation of state and sound velocity of a helium plasma by thomas-fermi-dirac molecular dynamics. *Physics of plasmas*, 13(9):092701, 2006.

[2] F. Lambert, J. Clérouin, and G. Zérah. Very-high-temperature molecular dynamics. *Phys. Rev. E*, 73:016403, 2006.

[3] J. D. Kress, James S. Cohen, D. P. Kilcrease, D. A. Horner, and L. A. Collins. Orbital-free molecular dynamics simulations of transport properties in dense-plasma uranium. *High Energy Density Physics*, 7(3):155–160, 2011.

[4] Jean Clérouin, Gregory Robert, Philippe Arnault, Joel D Kress, and Lee A Collins. Behavior of the coupling parameter under isochoric heating in a high-z plasma. *Physical Review E*, 87(6):061101, 2013.

[5] J. Clerouin, E. L. Pollock, and G. Zerah. Thomas-fermi molecular dynamics. *Physical Review A*, 46(8):5130, 1992.

[6] T. G. White, S. Richardson, B. J. B. Crowley, L. K. Pattison, J. W. O. Harris, and G. Gregori. Orbital-free density-functional theory simulations of the dynamic structure factor of warm dense aluminum. *Physical review letters*, 111(17):175002, 2013.

[7] Valentin V. Karasiev, Travis Sjostrom, and Samuel B. Trickey. Finite-temperature orbital-free dft molecular dynamics: Coupling profess and quantum espresso. *Computer Physics Communications*, 185(12):3240–3249, 2014.

[8] N. David Mermin. Thermal properties of the inhomogeneous electron gas. *Phys. Rev.*, 137:A1441–A1443, Mar 1965.

[9] C. E. Starrett and D. Saumon. Electronic and ionic structures of warm and hot dense matter. *Phys. Rev. E*, 87:013104, Jan 2013.

[10] Paul A.M. Dirac. Note on exchange phenomena in the thomas atom. *Proceedings of the Cambridge Philosophical Society*, 26:376, 1930.

[11] Libero J. Bartolotti and Robert G. Parr. The concept of pressure in density functional theory. *The Journal of Chemical Physics*, 72(3):1593–1596, 1980.

[12] C.E. Starrett and D. Saumon. A simple method for determining the ionic structure of warm dense matter. *High Energy Density Physics*, 10(0):35 – 42, 2014.

[13] C. E. Starrett, D. Saumon, J. Daligault, and S. Hamel. Integral equation model for warm and hot dense mixtures. *Phys. Rev. E*, 90:033110, Sep 2014.

[14] C. E. Starrett and D. Saumon. Equation of state of dense plasmas with pseudoatom molecular dynamics. *Phys. Rev. E*, 93:063206, Jun 2016.

[15] J. Bernal. Fortran codes for voronoi tesselation and delauney triangulations, nist math webpages. http://math.nist.gov/jbernal/jbernal_sft.html.

[16] Aftab Alam, S. N. Khan, Brian G. Wilson, and D. D. Johnson. Efficient isoparametric integration over arbitrary space-filling voronoi polyhedra for electronic structure calculations. *Phys. Rev. B*, 84:045105, Jul 2011.

[17] Gregory S. Ho, Vincent L. Lignères, and Emily A. Carter. Introducing profess: A new program for orbital-free density functional theory calculations. *Computer physics communications*, 179(11):839–854, 2008.

[18] Paul P. Ewald. Die berechnung optischer und elektrostatischer gitterpotentiale. *Annalen der Physik*, 369(3):253–287, 1921.

[19] C. E. Starrett, J. Daligault, and D. Saumon. Pseudoatom molecular dynamics. *Phys. Rev. E*, 91:013104, Jan 2015.

[20] R. P. Feynman, N. Metropolis, and E. Teller. Equations of state of elements based on the generalized fermi-thomas theory. *Phys. Rev.*, 75:1561–1573, May 1949.

[21] Travis Sjostrom and Jérôme Daligault. Fast and accurate quantum molecular dynamics of dense plasmas across temperature regimes. *Phys. Rev. Lett.*, 113:155006, Oct 2014.